

Magnetism: Molecules to Materials V

Edited by Joel S. Miller and Marc Drillon



WILEY-
VCH

WILEY-VCH Verlag GmbH Co. KGaA

Magnetism: Molecules to Materials V

Edited by J.S. Miller and M. Drillon

Further Titles of Interest:

J.S. Miller, M. Drillon (Eds.)

Magnetism: Molecules to Materials IV

2003, ISBN 3-527-30429-0

J.S. Miller, M. Drillon (Eds.)

Magnetism: Molecules to Materials III

Nanosized Magnetic Materials

2002, ISBN 3-527-30302-2

J.S. Miller, M. Drillon (Eds.)

Magnetism: Molecules to Materials II

Molecule-Based Materials

2001, ISBN 3-527-30301-4

J.S. Miller, M. Drillon (Eds.)

Magnetism: Molecules to Materials

Models and Experiments

2001, ISBN 3-527-29772-3

F. Schüth, K.S.W. Sing, J. Weitkamp (Eds.)

Handbook of Porous Solids

2002, ISBN 3-527-30246-8

F. Laeri, F. Schüth, U. Simon, M. Wark (Eds.)

Host-Guest-Systems Based on Nanoporous Crystals

2003, ISBN 3-527-30501-7

Magnetism: Molecules to Materials V

Edited by Joel S. Miller and Marc Drillon



WILEY-
VCH

WILEY-VCH Verlag GmbH Co. KGaA

Prof. Dr. Joel S. Miller
Department of Chemistry
University of Utah
Salt Lake City
UT 84112-0850
USA

Prof. Dr. Marc Drillon
CNRS
Institut de Physique et Chimie
des Matériaux de Strasbourg
23 Rue du Loess
67037 Strasbourg Cedex
France

All books published by Wiley-VCH are carefully produced. Nevertheless, authors, editors, and publisher do not warrant the information contained in these books, including this book, to be free of errors. Readers are advised to keep in mind that statements, data, illustrations, procedural details or other items may inadvertently be inaccurate

Library of Congress Card No.: Applied for

British Library Cataloguing-in-Publication Data:

A catalogue record for this book is available from the British Library

Bibliographic information published by

Die Deutsche Bibliothek

Die Deutsche Bibliothek lists this publication in the Deutsche Nationalbibliografie; detailed bibliographic data is available in the

Internet at <<http://dnb.ddb.de>>

© 2005 WILEY-VCH Verlag GmbH & Co. KGaA, Weinheim

All rights reserved (including those of translation into other languages). No part of this book may be reproduced in any form – by photoprinting, microfilm, or any other means – nor transmitted or translated into a machine language without written permission from the publishers. Registered names, trademarks, etc. used in this book, even when not specifically marked as such, are not to be considered unprotected by law.

Printed in the Federal Republic of Germany
Printed on acid-free and chlorine-free paper

Composition: EDV-Beratung Frank Herweg, Leutershausen
Printing: betz-druck gmbh, Darmstadt
Bookbinding: Litges & Dopf Buchbinderei, Heppenheim

ISBN: 3-527-30665-X

Contents

Preface	XI
1 Metalloceonium Salts of Radical Anion Bis(Dichalcogenate) Metalates <i>Vasco Gama and Maria Teresa Duarte</i>	1
1.1 Introduction	1
1.2 Basic Structural Motifs	4
1.2.1 ET Salts Based on Decamethylmetalloceonium Donors	4
1.2.2 ET Salts Based on Other Metalloceonium Donors	6
1.3 Solid-state Structures and Magnetic Behavior	7
1.3.1 Type I Mixed Chain Salts	7
1.3.2 Type II Mixed Chain $[M(Cp^*)_2][M'(L)_2]$ Salts	21
1.3.3 Type III Mixed Chain $[M(Cp^*)_2][M'(L)_2]$ Salts	23
1.3.4 Type IV Mixed Chain $[M(Cp^*)_2][M'(L)_2]$ Salts	30
1.3.5 Salts with Segregated Stacks not 1D Structures	36
1.4 Summary and Conclusions	37
References	39
2 Chiral Molecule-Based Magnets <i>Katsuya Inoue, Shin-ichi Ohkoshi, and Hiroyuki Imai</i>	41
2.1 Introduction	41
2.2 Physical and Optical Properties of Chiral or Noncentrosymmetric Magnetic Materials	41
2.2.1 Magnetic Structure and Anisotropy	42
2.2.2 Nonlinear Magneto-optical Effects	43
2.2.3 Magneto-chiral Optical Effects	48
2.3 Nitroxide-manganese Based Chiral Magnets	49
2.3.1 Crystal Structures	49
2.3.2 Magnetic Properties	51
2.4 Two- and Three-dimensional Cyanide Bridged Chiral Magnets	53
2.4.1 Crystal Design	54
2.4.2 Two-dimensional Chiral Magnet [39]	54
2.4.3 Three-dimensional Chiral Magnet [40]	57

2.4.4	Conclusion	60
2.5	SHG-active Prussian Blue Magnetic Films	60
2.5.1	Magnetic Properties and the Magneto-optical Effect	60
2.5.2	Nonlinear Magneto-optical Effect	64
2.6	Conclusion	68
	References	69
3	Cooperative Magnetic Behavior in Metal-Dicyanamide Complexes	
	<i>Jamie L. Manson</i>	71
3.1	Introduction	71
3.2	“Binary” α -M(dca) ₂ Magnets	73
3.2.1	Structural Aspects	73
3.2.2	Ferromagnetism	76
3.2.3	Canted Antiferromagnetism	79
3.2.4	Mechanism for Magnetic Ordering	81
3.2.5	Pressure-dependent Susceptibility	82
3.3	β -M(dca) ₂ Magnets	82
3.3.1	Structural Evidence	82
3.3.2	Magnetic Behavior of α -Co(dca) ₂	84
3.3.3	Comparison of Lattice and Spin Dimensionality in α - and β -Co(dca) ₂	85
3.4	Mixed-anion M(dca)(tcm)	85
3.4.1	Crystal Structure	85
3.4.2	Magnetic Properties	86
3.5	Polymeric 2D (cat)M(dca) ₃ cat = Ph ₄ As, Fe(bipy) ₃	87
3.5.1	(Ph ₄ As)[Ni(dca) ₃]	87
3.5.2	[Fe(bipy) ₃][M(dca) ₃] ₂ {M = Mn, Fe}	88
3.6	Heteroleptic M(dca) ₂ L Magnets	88
3.6.1	Mn(dca) ₂ (pyz)	89
3.6.2	Mn(dca) ₂ (2,5-Me ₂ pyz) ₂ (H ₂ O) ₂	95
3.6.3	Mn(dca) ₂ (H ₂ O)	96
3.6.4	Fe(dca) ₂ (pym)-EtOH	97
3.6.5	Fe(dca) ₂ (abpt) ₂	98
3.7	Dicyanophosphide: A Phosphorus-containing Analog of Dicyanamide	99
3.8	Conclusions and Future Prospects	100
	References	101
4	Molecular Materials Combining Magnetic and Conducting Properties	
	<i>Peter Day and Eugenio Coronado</i>	105
4.1	Introduction	105
4.2	Interest of Conducting Molecular-based Magnets	106

4.2.1	Superconductivity and Magnetism	107
4.2.2	Exchange Interaction between Localised Moments and Conduction Electrons	108
4.3	Magnetic Ions in Molecular Charge Transfer Salts	111
4.3.1	Isolated Magnetic Anions	111
4.3.2	Metal Cluster Anions	131
4.3.3	Chain Anions: Maleonitriledithiolates	143
4.3.4	Layer Anions: Tris-oxalatometallates	146
4.4	Conclusions	153
	References	155
5	Lanthanide Ions in Molecular Exchange Coupled Systems	
	<i>Jean-Pascal Sutter and Myrtil L. Kahn</i>	161
5.1	Introduction	161
5.1.1	Generalities	161
5.2	Molecular Compounds Involving Gd(III)	164
5.2.1	Gd(III)–Cu(II) Systems	164
5.2.2	Systems with Other Paramagnetic Metal Ions	165
5.2.3	Gd(III)-organic Radical Compounds	165
5.3	Superexchange Mediated by Ln(III) Ions	170
5.4	Exchange Coupled Compounds Involving Ln(III) Ions with a First-order Orbital Momentum	174
5.4.1	Qualitative Insight into the Exchange Interaction	174
5.4.2	Quantitative Insight into the Exchange Interaction	180
5.4.3	The Exchange Interaction	181
5.5	Concluding Remarks	185
	References	185
6	Monte Carlo Simulation: A Tool to Analyse Magnetic Properties	
	<i>Joan Cano and Yves Journaux</i>	189
6.1	Introduction	189
6.2	Monte Carlo Method	190
6.2.1	Generalities	190
6.2.2	Metropolis Algorithm	192
6.2.3	Thermalization Process	193
6.2.4	Size of Model and Periodic Boundary Conditions	194
6.2.5	Random Number Generators	196
6.2.6	Magnetic Models	196
6.2.7	Structure of a Monte Carlo Program	197
6.3	Regular Infinite Networks	199
6.4	Alternating Chains	203
6.5	Finite Systems	206
6.6	Exact Laws versus MC Simulations	208

6.6.1	A Method to Obtain an ECS Law for a Regular 1D System: Fisher's Law	209
6.6.2	Small Molecules	211
6.6.3	Extended Systems	213
6.7	Some Complex Examples	217
6.8	Conclusions and Future Prospects	220
	References	220
7	Metalloocene-based Magnets	
	<i>Gordon T. Yee and Joel S. Miller</i>	223
7.1	Introduction	223
7.2	Electrochemical and Magnetic Properties of Neutral Decamethylmetallocenes and Decamethylmetallocenium Cations Paired with Diamagnetic Anions	224
7.3	Preparation of Magnetic Electron Transfer Salts	226
7.3.1	Electron Transfer Routes	226
7.3.2	Metathetical Routes	226
7.4	Crystal Structures of Magnetic ET Salts	227
7.5	Tetracyanoethylene Salts (Scheme 7.2)	230
7.5.1	Iron	230
7.5.2	Manganese	232
7.5.3	Chromium	232
7.5.4	Other Metals	232
7.6	Dimethyl Dicyanofumarate and Diethyl Dicyanofumarate Salts	233
7.6.1	Manganese	233
7.6.2	Chromium	234
7.7	2,3-Dichloro-5,6-dicyanoquinone Salts and Related Compounds	235
7.8	2,3-Dicyano-1,4-naphthoquinone Salts	236
7.8.1	Iron	236
7.8.2	Manganese	237
7.8.3	Chromium	238
7.9	7,7,8,8-Tetracyano- <i>p</i> -quinodimethane Salts	238
7.9.1	Iron	238
7.9.2	Manganese	239
7.9.3	Chromium	239
7.10	2,5-Dimethyl- <i>N, N'</i> -dicyanoquinodiimine Salts	239
7.10.1	Iron and Manganese	239
7.11	1,4,9,10-Anthracenetetrone Salts	240
7.12	Cyano and Perfluoromethyl Ethylenedithiolato Metalate Salts	240
7.12.1	Iron	241
7.12.2	Manganese	241

7.13	Benzenedithiolates and Ethylenedithiolates	244
7.14	Additional Dithiolate Examples	245
7.15	Bis(trifluoromethyl)ethylenediselenato Nickelate Salts	246
7.16	Other Acceptors that Support Ferromagnetic Coupling, but not Long-range Order above ~ 2 K	246
7.17	Other Metallocenes and Related Species as Donors	249
7.18	Muon Spin Relaxation Spectroscopy	251
7.19	Mössbauer Spectroscopy	251
7.20	Spin Density Distribution from Calculations and Neutron Diffraction Data	253
7.21	Dimensionality of the Magnetic System and Additional Evidence for a Phase Transition	253
7.22	The Controversy Around the Mechanism of Magnetic Coupling in ET Salts	254
7.23	Trends	255
7.24	Research Opportunities	256
	References	257
8	Magnetic Nanoporous Molecular Materials	
	<i>Daniel Maspoch, Daniel Ruiz-Molina, and Jaume Veciana</i>	261
8.1	Introduction	261
8.2	Inorganic and Molecular Hybrid Magnetic Nanoporous Materials	263
8.3	Magnetic Nanoporous Coordination Polymers	266
	8.3.1 Carboxylic Ligands	266
	8.3.2 Nitrogen-based Ligands	271
	8.3.3 Paramagnetic Organic Polytopic Ligands	273
8.4	Summary and Perspectives	278
	References	280
9	Magnetic Prussian Blue Analogs	
	<i>Michel Verdaguer and Gregory S. Girolami</i>	283
9.1	Introduction	283
9.2	Prussian Blue Analogs (PBA), Brief History, Synthesis and Structure	284
	9.2.1 Formulation and Structure	285
	9.2.2 Synthesis	288
9.3	Magnetic Prussian Blues (MPB)	290
	9.3.1 Brief Historical Survey of Magnetic Prussian Blues	291
	9.3.2 Interplay between Models and Experiments	293
	9.3.3 Quantum Calculations	306
9.4	High T_C Prussian Blues (the Experimental Race to High Curie Temperatures)	322
	9.4.1 Chromium(II)–Chromium(III) Derivatives	323

9.4.2	Manganese(II)–Vanadium(III) Derivatives	324
9.4.3	The Vanadium(II)–Chromium(III) Derivatives	325
9.4.4	Prospects in High- T_C Magnetic Prussian Blues	334
9.5	Prospects and New Trends	338
9.5.1	Photomagnetism: Light-induced Magnetisation	338
9.5.2	Fine Tuning of the Magnetisation	339
9.5.3	Dynamics in Magnetic and Photomagnetic Prussian Blues	339
9.5.4	Nanomagnetism	339
9.5.5	Blossoming of Cyanide Coordination Chemistry	340
9.6	Conclusion: a 300 Years Old “Inorganic Evergreen”	341
	References	341
10	Scaling Theory Applied to Low Dimensional Magnetic Systems	
	<i>Jean Souletie, Pierre Rabu, and Marc Drillon</i>	347
10.1	Introduction	347
10.2	Non-critical-scaling: the Other Solutions of the Scaling Model	348
10.3	Universality Classes and Lower Critical Dimensionality	351
10.4	Phase Transition in Layered Compounds	352
10.5	Description of Ferromagnetic Heisenberg Chains	363
	10.5.1 Application to Ferromagnetic $S = 1$ Chains	366
10.6	Application to the Spin-1 Haldane Chain	368
10.7	Conclusion	375
	References	375
	Index	379

Preface

The development, characterization, and technological exploitation of new materials, particularly as components in ‘smart’ systems, are key challenges for chemistry and physics in the next millennium. New substances and composites including nanostructured materials are envisioned for innumerable areas including magnets for the communication and information sector of our economy. Magnets are already an important component of the economy with worldwide sales exceeding \$30 billion per annum. Hence, research groups worldwide are targeting the preparation and study of new magnets especially in combination with other technologically important properties, *e. g.*, electrical and optical properties.

In the past few years our understanding of magnetism and magnetic materials, thought to be mature, has enjoyed a renaissance as it is being expanded by contributions from many diverse areas of science and engineering. These include (i) the discovery of bulk ferro- and ferrimagnets based on organic/molecular components with critical temperature exceeding room temperature, (ii) the discovery that clusters in high, but not necessarily the highest, spin states due to a large magnetic anisotropy or zero field splitting have a significant relaxation barrier that traps magnetic flux enabling a single molecule/ion (cluster) to act as a magnet at low temperature; (iii) the discovery of materials exhibiting large, negative magnetization; (iv) spin-crossover materials that can show large hysteretic effects above room temperature; (v) photomagnetic and (vi) electrochemical modulation of the magnetic behavior; (vii) the Haldane conjecture and its experimental realization; (viii) quantum tunneling of magnetization in high spin organic molecules; (ix) giant and (x) colossal magnetoresistance effects observed for 3-D network solids; (xi) the realization of nanosize materials, such as self organized metal-based clusters, dots and wires; (xii) the development of metallic multilayers and the spin electronics for the applications. This important contribution to magnetism and more importantly to science in general will lead us into the next millennium.

Documentation of the status of research, ever since William Gilbert’s *de Magnete* in 1600, provides the foundation for future discoveries to thrive. As this millennium begins the time is appropriate to pool our growing knowledge and assess many aspects of magnetism. This series entitled *Magnetism: Molecules to Mate-*

rials provides a forum for comprehensive yet critical reviews on many aspects of magnetism that are on the forefront of science today.

Joel S. Miller
Salt Lake City

Marc Drillon
Strasbourg, France

List of Contributors

Joan Cano
Laboratoire de Chimie Moléculaire
Université de Paris-Sud
91405 Orsay
France

Eugenio Coronado
Instituto de Ciencia Molecular
Universitat de Valencia
C/ Doctor Moliner 50
46100 Burjassot
Spain

Vasco Pires Silva da Gama
Instituto Tecnológico e Nuclear
Estrada Nacional 10
2686-953 Sacavém
Portugal

Peter Day
Davy Faraday Research Laboratory
The Royal Institution of Great Britain
21 Albemarle Street
London W1S 4BS
United Kingdom

Marc Drillon
Institut de Physique et Chimie
des Matériaux de Strasbourg
UMR 7504 du CNRS
23 Rue du Loess
67037 Strasbourg
France

Maria Teresa Duarté
Centro de Química Estrutural
Instituto Superior Técnico
Av. Rovisco Pais
1049-001 Lisboa
Portugal

Gregory S. Girolami
Department of Chemistry
University of Illinois
Urbana-Champaign 61801
USA

Hiroyuki Imai
Institute for Molecular Science
Okazaki National Institutes
38 Nishigounaka
Myoudaiji
Okazaki 444-8585
Japan

Katsuya Inoue
Institute for Molecular Science
Okazaki National Institutes
38 Nishigounaka
Myoudaiji
Okazaki 444-8585
Japan

Yves Journaux
Laboratoire de Chimie Inorganique,
URA 420
Université de Paris-Sud
CNRS, BAT 420
91405 Orsay
France

Myrtil L. Kahn
Institut de Chimie
de la Matière Condensée
de Boreaux – CNRS
Avenue Dr. Schweitzer
33608 Pessac
France

Jamie L. Manson
Department of Chemistry
and Biochemistry
Eastern Washington University
226 Science
526 5th St.
Cheney, WA 99004
USA

Daniel Maspoch
Institut de Ciència de Materials
de Barcelona (CSIC)
Campus Universitari de Bellaterra
08193 Cerdanyola
Spain

Joel S. Miller
Department of Chemistry
University of Utah
Salt Lake City, UT 84112-0850
USA

Shin-ichi Ohkoshi
Research Center for Advanced Science
and Technology
The University of Tokyo
4-6-1 Komaba
Meguro-ku
Tokyo 153-8904
Japan

Daniel Ruiz-Molina
Institut de Ciència de Materials
de Barcelona (CSIC)
Campus Universitari de Bellaterra
08193 Cerdanyola
Spain

Pierre Rabu
Institut de Physique et Chimie
des Matériaux de Strasbourg
UMR 75040 du CNRS
23 rue du Loess
67037 Strasbourg
France

Jean Souletie
Centre de Recherche sur les très
basses températures, CNRS
25 Avenue des Martyrs
38042 Grenoble
France

Jean-Pascal Sutter
Institut de Chimie
de la Matière Condensée
de Bordeaux – CNRS
Avenue Dr. Schweitzer
33608 Pessac
France

Jaume Veciana
Institut de Ciència de Materials
de Barcelona (CSIC)
Campus Universitari de Bellaterra
08193 Cerdanyola
Spain

Michel Verdaguer
Laboratoire de Chimie Inorganique
et Matériaux Moléculaires
Unité associée au C.N.R.S. 7071
Université Pierre et Marie Curie
4 place Jussieu
75252 Paris Cedex 05
France

Gordon T. Yee
Department of Chemistry
Virginia Polytechnic Institute
and State University
Blacksburg, VA 24061
USA

1 Metallocenium Salts of Radical Anion Bis(Dichalcogenate) Metalates

Vasco Pires Silva da Gama and Maria Teresa Duarte

1.1 Introduction

For the last 30 years metal-bis(1,2-dichalcogenate) anionic complexes have been extensively used as building blocks for the preparation of both conducting and magnetic molecular materials. Several of these materials show remarkable features and have made a significant contribution to the development of molecular materials science.

It is worth mentioning some examples of the molecular materials based on metal-bis(1,2-dichalcogenate) anionic complexes based that have made a significant contribution to the field of molecular material science, in the last decades. A large number of molecular conductors and even superconductors based on metal-bis(1,2-dichalcogenate) anionic acceptors have been obtained [1] and $\text{Me}_4\text{N}[\text{Ni}(\text{dmit})_2]_2$ (dmit = 1,3-dithiol-2-thione-4,5-dithiolate) was the first example of a π acceptor superconductor with a closed-shell donor [2]. The spin-Peierls transition was observed for the first time in the linear spin chain system $\text{TTF}[\text{Cu}(\text{tdt})_2]$ [3] (TTF = tetrathiafulvalene; tdt = 1,2-ditrifluoromethyl-1,2-ethylenedithioate). The co-existence of linear spin chains and conducting electrons, was observed for the first time in the compounds $\text{Per}_2[\text{M}(\text{mnt})_2]$ (M = Ni, Pd, Pt) [4] (mnt = 1,2-dicyano-1,2-ethylene-dithiolato), presenting competing spin-Peierls and Peierls instabilities of the spin chains and 1D conducting electronic systems. A purely organic system with a spin-ladder configuration was observed for the first time in the compound $\text{DT-TTF}_2[\text{Au}(\text{mnt})_2]$ [5] (DT-TTF = dithiophentetrathiafulvalene). A spin transition was observed in the compound $[\text{Fe}(\text{mnt})_2\text{rad}]$ [6], where rad = 2-(*p*-*N*-methylpyridinium)4,4,5,5-tetramethylimidazoline-1-oxyl. Ferromagnetic ordering was reported for $\text{NH}_4[\text{Ni}(\text{mnt})_2]\text{H}_2\text{O}$ [7].

The discovery of the first molecule-based material exhibiting ferromagnetic ordering, the electron-transfer (ET) salt $[\text{Fe}(\text{Cp}^*)_2]\text{TCNE}$ (TCNE = tetracyanoethylene), with $T_C = 4.8$ K, in 1986 [8, 9], was a landmark in molecular magnetism and gave a significant impulse to this field. Since then among the strategies followed to obtain cooperative magnetic properties, considerable attention has been given to the linear-chain electron-transfer salts based on metallocenium donors and on planar acceptors. [10, 11]. Besides $[\text{Fe}(\text{Cp}^*)_2]\text{TCNE}$, bulk ferromagnetism was reported

for other ET salts based on decamethylmetallocenes and on the conjugated polynitriles TCNE [12] and TCNQ [13] (TCNQ = 7,7,8,8-tetracyano-*p*-quinodimethane). An extensive study of these salts was made, covering a variety of aspects including the structure-magnetic property relationship [10], and the effects of spin variation and of spinless defects [10]. Furthermore they provided a valuable basis to test the various models that were proposed in order to explain the magnetic coupling and magnetic ordering in the molecule-based magnets [14, 15].

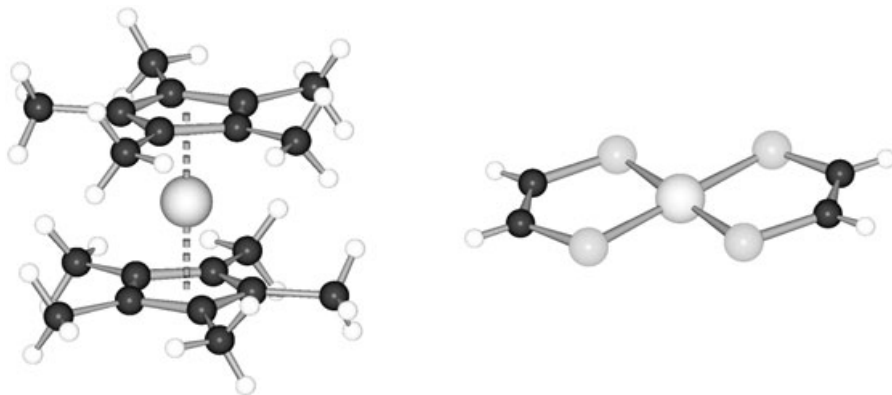
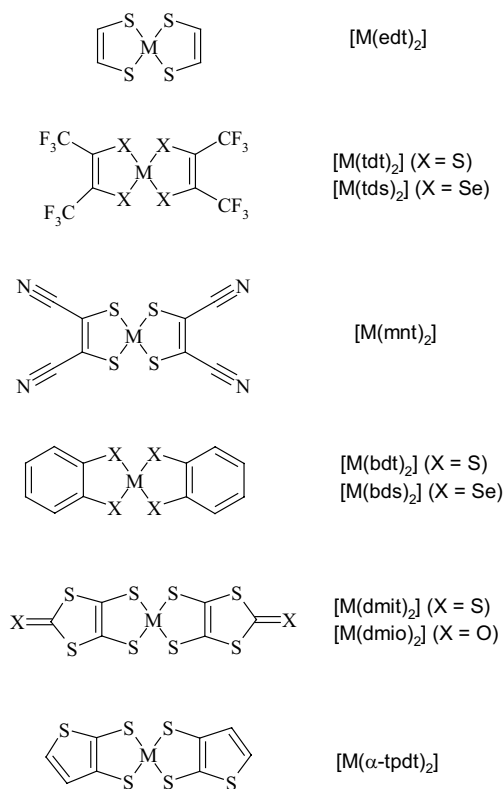


Fig. 1.1. Molecular structure of $[\text{Fe}(\text{Cp}^*)_2][\text{Ni}(\text{edt})_2]$, showing the basic donor and acceptor molecules studied in this review.

Following the report of ferromagnetism for $[\text{Fe}(\text{Cp}^*)_2]\text{TCNE}$, metal bis-dichalcogenate planar acceptors were also considered as suitable candidates for use in the preparation of ET salts with the radical metallocenium donors, and in the search for new molecular magnets the first metal bis-dichalcogenate based compounds were reported in 1989 [16, 17]. In particular the monoanionic forms of the metal bis-dichalcogenate (Ni, Pd, Pt) complexes seem particularly promising for “the synthesis of mixed-stack molecular charge-transfer salts that display cooperative magnetic phenomena due to (1) their planar structures, (2) delocalized electronic states, $S = 1/2$ spin state for the monomeric species, and (3) the possibility of extended magnetic interactions mediated by the chalcogen atoms” [17].

The work with ET salts based on metallocenium donors and on planar metal bis-dichalcogenate radical anions is summarized in this chapter. Most of the materials studied to date are decamethylmetallocenium based ET salts, other compounds based on different metallocenium derivatives have also been reported and will be



Scheme 1.1 Schematic representation of the metal bis-dichalcogenate acceptors studied in this chapter.

referred to. The metal bis-dichalcogenate complexes mentioned in this chapter are represented in Scheme 1.1.

As magnetic ordering is a bulk property, particular attention will be given to the supramolecular arrangements which determine the magnetic behavior. The crystal structure of the compounds will be correlated with the magnetic behavior of these ET salts. The magnetic coupling in the ET salts based on decamethylmetalloccenium donors has been analyzed mainly through McConnell I [18] or McConnell II [19] mechanisms, and this issue is still a subject of controversy [15, 20]. Of these models, McConnell I has been most often used in the interpretation of the magnetic behavior of these salts, as, in spite of its simplicity, it has shown good agreement with the experimental observations. In this chapter the interpretation of the magnetic coupling will be analyzed in the perspective of this model. However, it should be mentioned that the validity of the McConnell I mechanism has been questioned both theoretically [21] and experimentally [22].

1.2 Basic Structural Motifs

1.2.1 ET Salts Based on Decamethylmetallocenium Donors

In most of the ET salts based on decamethylmetallocenium donors, due to the planar configurations of both the C_5Me_5 ligands and of the metal bis-dichalcogenate acceptors the crystal structures are, with a few exceptions, based on linear chain arrangements of alternating donor and acceptor molecules. In these salts four distinct types of linear chain arrangements have been observed and are represented schematically in Figure 1.2. The type I chain arrangement corresponds to the most simple case of an alternated linear chain motif $\cdots A^- D^+ A^- D^+ A^- D^+ \cdots$, similar to that observed in several salts based on metallocenium donors and on acceptors such as TCNE and TCNQ [10]. In the case of the type II chain, the donors alternate with face-to-face pairs of acceptors, $\cdots A^- A^- D^+ A^- A^- D^+ \cdots$, as in this arrangement there is a net charge ($-$) per repeat unit, $A^- A^- D^+$, charge compensation is required. For the type III arrangement the linear chains consist of alternated face-to-face pairs of acceptors with side-by-side pairs of donors, $\cdots A^- A^- D^+ D^+ A^- A^- D^+ D^+ \cdots$. Finally in the type IV arrangement, the acceptors alternate with side-by-side pairs of donors, $\cdots A^- D^+ D^+ A^- D^+ D^+ \cdots$, in this case there is a net charge ($+$) per repeat unit, $D^+ D^+ A^-$, which must be compensated. For most of the ET salts based on types I and III arrangements (neutral chains), only one type of chain arrangement was observed. However, in the case of compounds based on types II and IV arrangements (charged chains), more complex crystal structures could be observed, resulting from the required charge neutralization. Table 1.1 summarizes the unit cell parameters, space group symmetry, and the type of observed linear chain ar-

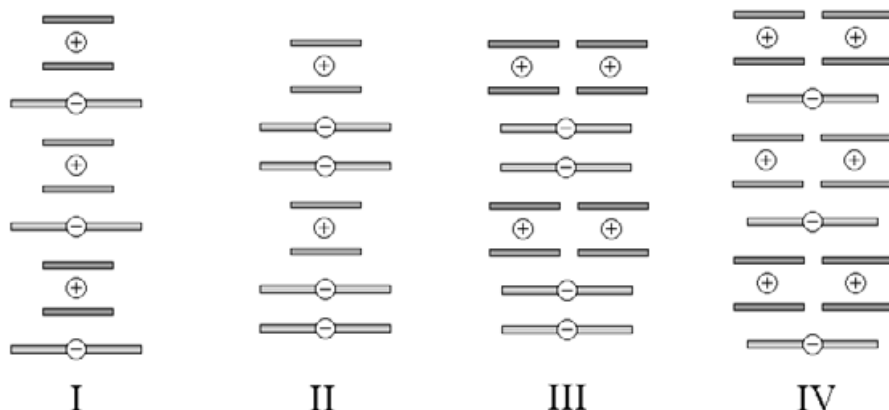


Fig. 1.2. Representation of the basic types of mixed chain sequences observed in the ET salts based on metallocene donors and on metal bis-dichalcogenate acceptors.

Table 1.1. Unit cell parameters and chain type for the mixed chain salts.

Compound	Chain Type	Space Group	<i>a</i> , Å	<i>b</i> , Å	<i>c</i> , Å	α , °	β , °	γ , °	Vol., Å ³	Z	<i>T</i> , °C	Ref.
[Fe(Cp [*]) ₂][Ni(edt) ₂]	I	C2/m	13.319	13.699	8.719	90.00	125.06	90.00	1302	2	20	23
[Cr(Cp [*]) ₂][Ni(edt) ₂]	I	C2/m	13.44	13.66	8.96	90.0	124.2	90.0	1320	2	20	23
[Fe(Cp [*]) ₂][Ni(tdt) ₂]	I	C2/c	14.417	12.659	18.454	90.00	95.17	90.00	3354	4	-70	16
[Mn(Cp [*]) ₂][Ni(tdt) ₂]	I	C2/c	14.302	12.697	18.415	90.00	94.63	90.00	3333	4	(a)	24
[Fe(Cp [*]) ₂][Pt(tdt) ₂]	I	P $\bar{1}$	8.490	10.278	10.936	106.79	103.95	101.98	846	1	-70	25
[Fe(Cp [*]) ₂][Ni(tds) ₂]	I	P $\bar{1}$	8.581	10.464	11.132	107.96	103.65	101.82	881	1	20	26
[Mn(Cp [*]) ₂][Ni(tds) ₂]	I	P $\bar{1}$	8.582	10.472	11.158	108.41	103.57	101.79	882	1	20	27
[Cr(Cp [*]) ₂][Ni(tds) ₂]	I	P $\bar{1}$	8.580	10.547	11.138	109.49	103.20	101.76	881	1	20	28
[Fe(Cp [*]) ₂][Pt(tds) ₂]	I	P $\bar{1}$	8.606	10.521	11.138	108.81	102.89	101.30	891	1	20	26
[Mn(Cp [*]) ₂][Pt(tds) ₂]	I	P $\bar{1}$	8.618	10.560	11.239	109.49	102.78	101.30	899	1	20	28
[Cr(Cp [*]) ₂][Pt(tds) ₂]	I	C2/c	11.352	21.848	14.969	90.00	103.73	90.00	3607	4	20	28
α -[Fe(Cp [*]) ₂][Pt(mnt) ₂]	II	C2/m	16.802	21.095	12.942	90.00	94.52	90.00	4473	6	20	16
β -[Fe(Cp [*]) ₂][Pt(mnt) ₂]	I	P $\bar{1}$	12.106	14.152	14.394	108.94	96.37	90.51	2312	3	23	16
[Fe(Cp [*]) ₂][Cu(mnt) ₂]	IV	P $\bar{1}$	9.713	11.407	11.958	100.90	113.20	92.66	1185	1	25	29
[Fe(Cp [*]) ₂][Ni(dmit) ₂]	III	P $\bar{1}$	11.347	14.958	10.020	97.68	94.36	109.52	1575	2	-120	17
[Mn(Cp [*]) ₂][Ni(dmit) ₂]	III	P $\bar{1}$	11.415	14.940	10.020	97.40	94.58	109.63	1582	2	(a)	30
α -[Fe(Cp [*]) ₂][Pd(dmit) ₂]	III	P $\bar{1}$	9.907	12.104	14.464	82.44	85.80	82.73	1703	2	20	31
[Fe(Cp [*]) ₂][Pt(dmit) ₂]	III	P $\bar{1}$	9.996	11.554	15.108	109.72	97.62	93.78	1616	2	20	31
[Fe(Cp [*]) ₂][Ni(dmio) ₂][MeCN]	IV	C2/m	16.374	10.84	19.530	90.00	88.02	90.00	3431	4	(a)	32
[Fe(Cp [*]) ₂][Pd(dmio) ₂]	III	P $\bar{1}$	14.133	14.620	16.055	88.43	80.25	86.38	3260	4	20	31
[Fe(Cp [*]) ₂][Pt(dmio) ₂]	III	P $\bar{1}$	14.133	14.620	16.055	88.43	80.25	86.38	3260	4	20	31
[Fe(Cp [*]) ₂][Ni(dsit) ₂]	III	P $\bar{1}$	9.650	11.439	16.643	71.14	73.24	89.72	1657	2	20	31
[Fe(Cp [*]) ₂][Ni(bdt) ₂]	IV	P $\bar{1}$	9.731	19.044	35.677	105.22	94.91	97.99	6266	8	20	33
[Mn(Cp [*]) ₂][Ni(bdt) ₂]	IV	P $\bar{1}$	9.760	19.101	35.606	105.02	94.72	98.15	6293	8	20	33
[Cr(Cp [*]) ₂][Ni(bdt) ₂]	IV	P $\bar{1}$	9.782	17.885	19.163	74.84	81.58	82.91	3189	4	20	33
[Mn(Cp [*]) ₂][Co(bdt) ₂]	IV	P $\bar{1}$	9.738	19.119	35.698	105.27	94.36	98.34	6298	8	20	33
[Cr(Cp [*]) ₂][Co(bdt) ₂]	IV	P $\bar{1}$	9.772	17.896	19.198	75.12	81.45	82.09	3191	4	20	33
[Fe(Cp [*]) ₂][Pt(bdt) ₂]	IV	P $\bar{1}$	7.763	19.126	35.564	104.50	95.26	97.87	6314	8	20	33
[Cr(Cp [*]) ₂][Pt(bdt) ₂]	IV	P $\bar{1}$	9.787	19.241	35.587	103.98	94.69	98.31	6387	8	20	33
[Fe(Cp [*]) ₂][Ni(bds) ₂][MeCN]	IV	P $\bar{1}$	11.720	16.282	9.606	100.66	106.03	81.75	1723	2	-120	17
[Fe(Cp [*]) ₂][Ni(α -tpdt) ₂]	I	P2 ₁ /c	20.360	10.237	15.443	90.00	107.54	90.00	3069	4	20	34
[Cr(Cp [*]) ₂][Ni(α -tpdt) ₂]	I	P2 ₁ /c	10.053	10.281	15.577	90.00	104.89	90.00	1556	2	20	35
[Fe(C ₅ Me ₄ SCMe ₃) ₂][Ni(mnt) ₂]	I	P $\bar{1}$	9.619	9.622	11.253	79.72	78.66	76.62	984	1	22	36
[Fe(C ₅ Me ₄ SCMe ₃) ₂][Pt(mnt) ₂]	I	P $\bar{1}$	9.591	9.681	11.252	78.17	78.47	77.38	984	1	22	36

(a) Not given.

rangements for mixed chain ET salts based on metallocenium donors and metal bis-dichalcogenate acceptors.

While in the case of the cyano radical based salts, most of the observed structures present a type I structural arrangement, in the case of the ET salts based on metal bis-dichalcogenate acceptors a much larger variety of arrangements was observed, as described above. The structural motifs in the [M(Cp^{*})₂][M'(L)₂] ET salts are primarily determined by factors such as the dimensions of the anionic metal bis-dichalcogenate complexes, the tendency of the acceptors to associate as dimers, the extent of the π system in the acceptor molecule, and the charge density distribution on the ligands.

In the case of the [M(edt)₂]⁻ based salts, with the smaller acceptor, the size of the acceptor is similar to the size of the C₅Me₅ ligand of the donor and only type I structural motifs (DADA chains) were observed. For the intermediate size

anionic complexes, $[M(\text{tdx})_2]^-$, $[M(\text{mnt})_2]$ and $[\text{Ni}(\alpha\text{-tpdt})_2]^-$, the most common structural motif obtained in ET salts based on those acceptors is also of type I. For the larger anionic complexes, $[M(\text{bdx})_2]^-$ and $[M(\text{dmix})_2]^-$, types III and IV chain arrangements were observed, in both cases acceptor molecules (type IV) or face-to-face pairs of acceptors (type III) alternate with side-by-side pairs of donors. The complexes $[M(\text{mnt})_2]^-$ and $[M(\text{dmix})_2]^-$, ($M = \text{Ni}, \text{Pd}$ and Pt), frequently undergo dimerization in the solid state [37], and they are the only acceptors where the chain arrangements have face-to-face pairs of acceptors (structural motifs II and III). The variety of structural arrangements observed in the $[M(\text{mnt})_2]^-$ based compounds can be related to both the large extent of the π system and the high charge density on the terminal nitrile groups [38], as well as to the tendency of these complexes to form dimers.

1.2.2 ET Salts Based on Other Metalloccenium Donors

Besides the decamethylmetalloccenium based salts, in the compounds based on other metalloccenium derivatives, mixed linear chain arrangements were only observed in the case of the salts $[\text{Fe}(\text{C}_5\text{Me}_4\text{SCMe}_3)_2][M(\text{mnt})_2]$, $M = \text{Ni}$ and Pt , which present type I structural motifs.

Some ET salts based on other metalloccenium derivatives and on the acceptors $[M(\text{mnt})_2]^-$ and $[M(\text{dmit})_2]^-$ ($M = \text{Ni}$ and Pt) have also been reported. In the case of these compounds, the crystal structure consists of segregated stacks of donors, $\cdot\cdot\text{D}^+\text{D}^+\text{D}^+\text{D}^+\cdot\cdot$, and acceptors, $\cdot\cdot\text{A}^-\text{A}^-\text{A}^-\text{A}^-\cdot\cdot$, which is a common situation in molecular materials, in particular in the case of molecular conductors. In spite of the fact that for most salts the dominant magnetic interactions between the metal bis-dichalcogenate units are antiferromagnetic, there are cases where the interactions are known to be ferromagnetic, as in the case of the compounds $n\text{-Bu}_4\text{N}[\text{Ni}(\alpha\text{-tpdt})_2]$ [34] and $\text{NH}_4[\text{Ni}(\text{mnt})_2](\text{H}_2\text{O})$, which was the first metal bis-dichalcogenate based material to present ferromagnetic ordering, with $T_C = 4.5 \text{ K}$ [7]. The unit cell parameters of the ferrocenium derivative salts with crystal structures based on segregated acceptor stacks are shown in Table 1.2.

Table 1.2. Unit cell parameters for the segregated stack salts.

Compound	Space Group	$a, \text{Å}$	$b, \text{Å}$	$c, \text{Å}$	$\alpha, ^\circ$	$\beta, ^\circ$	$\gamma, ^\circ$	Vol., Å^3	Z	$T, ^\circ\text{C}$	Ref.
$[\text{Fe}(\text{Cp})_2]_2[\text{Ni}(\text{mnt})_2]_2[\text{Fe}(\text{Cp})_2]$	$P\bar{1}$	12.030	13.652	15.462	87.91	77.62	72.56	2365	2	(a)	39
$[\text{Fe}(\text{C}_5\text{Me}_4\text{SMe})_2][\text{Ni}(\text{mnt})_2]$	$P\bar{1}$	8.649	14.080	15.358	65.27	77.77	80.78	1654	2	22	36
$[\text{Fe}(\text{C}_5\text{H}_4\text{R})_2][\text{Ni}(\text{mnt})_2]$ (b)	$P2_1/n$	7.572	28.647	16.374	90.00	93.10	90.00	3547	4	22	40
$[\text{Fe}(\text{Cp})(\text{C}_5\text{H}_4\text{CH}_2\text{NMe}_3)][\text{Ni}(\text{mnt})_2]$	$P2_1/n$	12.116	30.094	7.139	90.00	103.97	90.00	2531	4	20	41
$[\text{Fe}(\text{Cp})(\text{C}_5\text{H}_4\text{CH}_2\text{NMe}_3)][\text{Pt}(\text{mnt})_2]$	$P2_1/n$	12.119	30.112	7.244	90.00	103.97	90.00	2565	4	20	41
$[\text{Co}(\text{Cp})_2][\text{Ni}(\text{dmit})_2]$	$P\bar{1}$	19.347	25.289	9.698	100.60	96.02	76.01	4517	8	20	42
$[\text{Co}(\text{Cp})_2][\text{Ni}(\text{dmit})_2]_2\text{2MeCN}$	$P\bar{1}$	8.913	21.370	7.413	99.19	91.06	101.40	1363	1	(a)	43

(a) Not given. (b) $[\text{Fe}(\text{C}_5\text{R})_2]^+ = 1,1'$ -bis[2-(4-(methylthio)-(E)-ethenyl)]ferrocenium.

1.3 Solid-state Structures and Magnetic Behavior

After listing the general characteristics of the crystal structures of ET salts based on metallocenium donors and metal bis-dichalcogenate acceptors, we will discuss them based on the systematization proposed in Section 1.2 and correlate the supramolecular crystal motifs with the magnetic properties.

1.3.1 Type I Mixed Chain Salts

The magnetic behavior of the salts based on type I chains shows a considerable similarity, namely, in most cases, the dominant magnetic interactions are FM and several of these salts exhibit metamagnetic behavior. Table 1.3 summarizes the key magnetic properties of type I compounds.

1.3.1.1 $[M(\text{Cp}^*)_2][\text{Ni}(\text{edt})_2]$

The compounds $[M(\text{Cp}^*)_2][\text{Ni}(\text{edt})_2]$, with $M = \text{Fe}$ and Cr , are isostructural and the crystal structure [23] consists of a parallel arrangement of 1D alternated type I chains, $\cdots\text{A}^-\text{D}^+\text{A}^-\text{D}^+\text{A}^-\text{D}^+\cdots$. In Figure 1.3(a) a view along the chain direction ([101]) is presented for $[\text{Fe}(\text{Cp}^*)_2][\text{Ni}(\text{edt})_2]$. The chains are regular and the Ni atoms sit above the Cp fragments from the donors, intrachain DA contacts, d ($d =$ interatomic separation), shorter than the sum of the van der Waals radii (d_w), $Q_w = d/d_w < 1$, were observed. These contacts involve a Ni atom from the acceptor and one of the C atoms from the C_5 ring, with a Ni–C distance of 3.678 Å ($Q_w = 0.99$). For this compound the shortest interchain interionic separation was found in the in-registry pair II–IV, with AA C–C contacts of 3.507 Å ($Q_w = 1.11$), as shown in Figure 1.3(b). The out-of-registry pairs I–II, II–III and I–IV present a similar interchain arrangement, with DA C–S contacts (C from Me from the donor and an S from the acceptor) of 3.812 Å ($Q_w = 1.11$), the II–III pairwise arrangement is shown in Figure 1.3(c).

At high temperatures, in the case of the $[M(\text{Cp}^*)_2][\text{Ni}(\text{edt})_2]$ compounds, AFM interactions apparently dominate the magnetic behavior of the compounds, as seen by the negative θ value obtained from the Curie–Weiss fits, -5 and -6.7 for $M = \text{Fe}$ and Cr respectively. A considerable field dependence of the obtained θ value for polycrystalline samples (free powder) was observed in the case of $[\text{Fe}(\text{Cp}^*)_2][\text{Ni}(\text{edt})_2]$, suggesting the existence of a strong anisotropy in the magnetic coupling for this compound [23]. This was confirmed by the metamagnetic behavior observed at low temperatures, with $T_N = 4.2$ K and $H_C = 14$ kG at 2 K.

A typical metamagnetic behavior was observed in single crystal magnetization measurements at 2 K [23], shown in Figure 1.4. With the applied magnetic field parallel to the chains a field induced transition from an AFM state to a high field FM

Table 1.3. Magnetic characterization of type I ET salts.

Compound	$S_D; S_A$	θ , K	Comments	Ref.
[Fe(Cp [*]) ₂][Ni(edt) ₂]	1/2; 1/2	-5	MM (a); $T_N = 4.2$ K; $H_C = 14$ kG (2 K)	23
[Cr(Cp [*]) ₂][Ni(edt) ₂]	3/2; 1/2	-6.7	(b)	23
[Fe(Cp [*]) ₂][Ni(tdt) ₂]	1/2; 1/2	15	(b)	16
[Mn(Cp [*]) ₂][Ni(tdt) ₂]	1; 1/2	2.6	MM (a); $T_N = 2.4$ K	24
[Mn(Cp [*]) ₂][Pd(tdt) ₂]	1; 1/2	3.7	MM (a); $T_N = 2.8$ K; $H_C = 0.8$ kG (1.85 K)	24
[Fe(Cp [*]) ₂][Pt(tdt) ₂]	1/2; 1/2	27	(b)	10
[Mn(Cp [*]) ₂][Pt(tdt) ₂]	1; 1/2	1.9	MM (a) $T_N = 2.3$ K;	24
[Fe(Cp [*]) ₂][Ni(tds) ₂]	1/2; 1/2	8.9	(b)	26, 44
[Mn(Cp [*]) ₂][Ni(tds) ₂]	1; 1/2	12.8	MM (a); $T_N = 2.1$ K; $H_C = 0.28$ kG (1.6 K)	28, 44
[Cr(Cp [*]) ₂][Ni(tds) ₂]	3/2; 1/2	4.0	(b)	28
[Fe(Cp [*]) ₂][Pt(tds) ₂]	1/2; 1/2	9.3	MM (a); $T_N = 3.3$ K; $H_C = 3.95$ kG (1.7 K)	26
[Mn(Cp [*]) ₂][Pt(tds) ₂]	1; 1/2	16.6	MM (a); $T_N = 5.7$ K; $H_C = 4.05$ kG (1.7 K)	28
[Cr(Cp [*]) ₂][Pt(tds) ₂]	3/2; 1/2	9.8	MM (c); $T_N = 5.2$ K; $H_{C1} = 5$ kG, $H_{C2} = 16$ kG, (1.7 K)	28
[Fe(Cp [*]) ₂][Ni(α -tpdt) ₂]	1/2; 1/2	-5.1 (d)	$T_m \approx 130$ K (e); MM (a); $T_N = 2.6$ K; $H_C = 0.6$ kG (1.6 K)	34
[Mn(Cp [*]) ₂][Ni(α -tpdt) ₂] (f)	1; 1/2	7.3	FM (g); $T_C = 2.2$ K	35
[Cr(Cp [*]) ₂][Ni(α -tpdt) ₂]	3/2; 1/2	6.1	(b)	35
[Fe(C ₅ Me ₄ SCMe ₃) ₂][Ni(mnt) ₂]	1/2; 1/2	3	(b)	36
[Fe(C ₅ Me ₄ SCMe ₃) ₂][Pt(mnt) ₂]	1/2; 1/2	3	(b)	36
β -[Fe(Cp [*]) ₂][Pt(mnt) ₂]	1/2; 1/2	9.8	(b)	16

(a) Metamagnetic transition. (b) No magnetic ordering observed down to 1.8 K. (c) Two field induced transitions were observed at low temperatures. (d) Non-Curie-Weiss behavior the given θ value relates to the high temperature region ($T > T_m$). (e) Minimum in χT vs. T . (f) Crystal structure not yet determined. (g) Ferromagnetic transition.

state occurs at a critical field of 14 kG. While for measurements with the applied field perpendicular to the chains, no transition was observed and a linear field dependence was observed for the magnetization, as expected for an AFM.

The magnetic behavior of [Fe(Cp^{*})₂][Ni(edt)₂] is consistent with the coexistence of FM intrachain interactions, due to DA intrachain short contacts, with AFM interchain interactions, resulting from the AD and AA interchain contacts. The nature of the intra and interchain magnetic interaction is in good agreement with the predictions of the McConnell I mechanism [26]. In this case the interchain interactions must be particularly large as they seem to be the dominant interactions

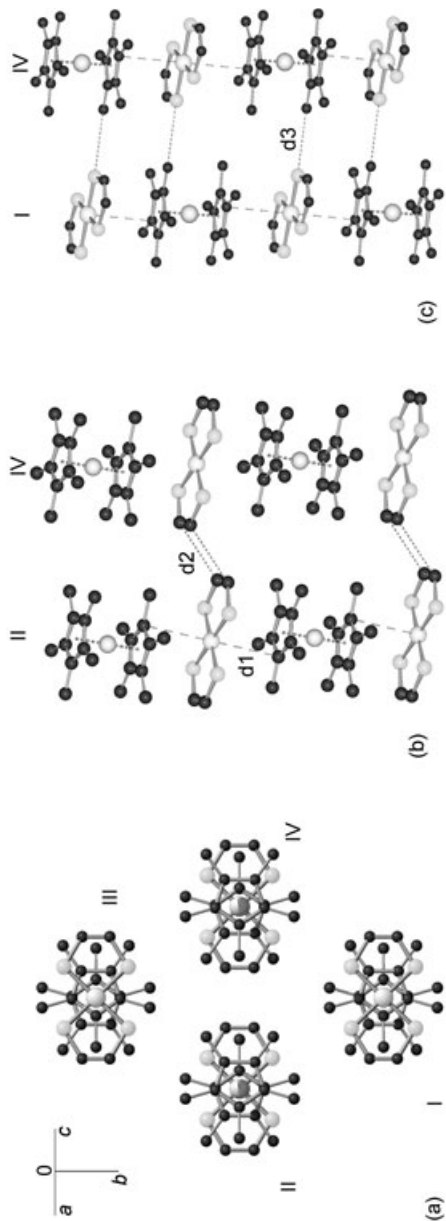


Fig. 1.3. (a) Perspective view of the crystal structure of $[\text{Fe}(\text{Cp}^*)_2][\text{Ni}(\text{edt})_2]$ along the chain direction. (b) Interchain arrangement of the pair II-I, $d1$ corresponds to the DA closest intrachain contact (3.678 Å, $Q_w = 0.99$) and $d2$ to the closest interchain contact (3.507 Å, $Q_w = 1.11$). (c) Interchain arrangement of the pair II-IV, $d3$ is the closest interchain contact (3.812 Å, $Q_w = 1.11$). Hydrogen atoms were omitted for clarity.

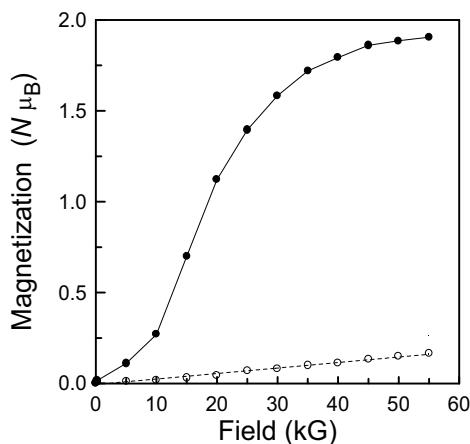


Fig. 1.4. Magnetization field dependence at 2 K, for a single crystal of $[\text{Fe}(\text{Cp}^*)_2][\text{Ni}(\text{edt})_2]$, the closed symbols refer to measurements with applied field parallel to the DADA chains and the open symbols to the measurements with the applied field perpendicular to the chains.

at high temperatures, and they also lead to a quite high value for the critical field in the metamagnetic transition.

1.3.1.2 $[\text{M}(\text{Cp}^*)_2][\text{M}'(\text{tdx})_2]$

The $[\text{Fe}(\text{Cp}^*)_2][\text{Ni}(\text{tdt})_2]$ and $[\text{Mn}(\text{Cp}^*)_2][\text{M}'(\text{tdt})_2]$ with $\text{M}' = \text{Ni}, \text{Pd}$ and Pt are isostructural, and, as in the case of the $[\text{M}(\text{Cp}^*)_2][\text{Ni}(\text{edt})_2]$ salts, a crystal structure based on an arrangement of parallel alternating DA linear chains [16] is observed, but with differences in the intra and interchain arrangements. A view normal to the chains of $[\text{Fe}(\text{Cp}^*)_2][\text{Ni}(\text{tdt})_2]$ is shown in Figure 1.5(a). In these compounds the chains have a zigzag arrangement and the Cp sits above one of the NiS_2C_2 fragments of the acceptor, as shown for $[\text{Fe}(\text{Cp}^*)_2][\text{Ni}(\text{tdt})_2]$ in Figure 1.5(b). In this compound, no intrachain DA short contacts were found and the closest interatomic separation between the acceptor and the Cp ring corresponds to Ni–C contacts of 4.120 \AA ($Q_{\text{W}} = 1.11$). In this salt the most relevant interchain contacts concern the out-of registry pairs I–II and I–IV, these arrangements are similar and the first one is shown in Figure 1.5(b). These pairs show interchain DA C–S contacts, involving C atoms of the Me groups of the donors and S atoms of the acceptors, with a separation of 3.728 \AA ($Q_{\text{W}} = 1.08$).

The magnetic behavior of the compounds $[\text{Fe}(\text{Cp}^*)_2][\text{Ni}(\text{tdt})_2]$ and $[\text{Mn}(\text{Cp}^*)_2][\text{M}'(\text{tdt})_2]$, with $\text{M}' = \text{Ni}, \text{Pd}$ and Pt , is dominated by the intrachain DA FM interactions, as seen by the positive θ values obtained from the Curie-Weiss fits (Table 1.3). At low temperatures the $[\text{Mn}(\text{Cp}^*)_2][\text{M}'(\text{tdt})_2]$ salts exhibit metamagnetic transitions, with $T_{\text{N}} = 2.4, 2.8$ and 2.3 K for $\text{M}' = \text{Ni}, \text{Pd}$ and Pt respectively, $H_{\text{C}} = 600 \text{ G}$ for $\text{M}' = \text{Pd}$ [24]. This behavior is attributed to the coexistence of FM intrachain interactions with interchain AFM interactions.

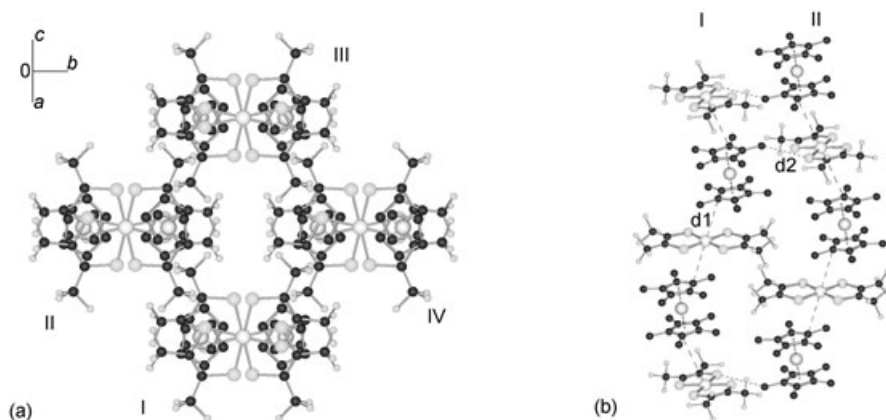


Fig. 1.5. (a) View of the crystal structure of $[\text{Fe}(\text{Cp}^*)_2][\text{Ni}(\text{tdt})_2]$ along the chain direction (Me groups were omitted for clarity). (b) Interchain arrangement of the pair I–II, d1 corresponds to the DA closest intrachain contact (4.120 Å, $Q_W = 1.11$) and d2 to the closest interchain contact (3.728 Å, $Q_W = 1.08$). Hydrogen atoms were omitted for clarity.

The compounds $[\text{Fe}(\text{Cp}^*)_2][\text{Pt}(\text{tdt})_2]$, $[\text{M}(\text{Cp}^*)_2][\text{Ni}(\text{tds})_2]$, with $\text{M} = \text{Fe}$, Mn and Cr , [25–28] and $[\text{M}(\text{Cp}^*)_2][\text{Pt}(\text{tds})_2]$, with $\text{M} = \text{Fe}$ and Mn , [26, 28] are isostructural and the crystal structure consists of a parallel arrangement of alternated type I chains. The intrachain arrangement is similar to that of $[\text{Fe}(\text{Cp}^*)_2][\text{Ni}(\text{edt})_2]$, with the Cp sitting above the Ni or Pt atoms from the acceptor, but distinct interchain arrangements were observed in these compounds. A view normal to the chains is shown in Figure 1.6(a) for $[\text{Fe}(\text{Cp}^*)_2][\text{Pt}(\text{tds})_2]$. Short intrachain DA contacts were observed in most of these salts, involving M (Ni or Pt) and carbons from the Cp rings from the donors, for the Pt–C contact in $[\text{Fe}(\text{Cp}^*)_2][\text{Pt}(\text{tds})_2]$ the interatomic separation is 3.826 Å ($Q_W = 0.98$). For this series of compounds the shortest interchain interionic separation was found in the in-registry pair I–II, shown in Figure 1.6(b), and it corresponds to an AA Se–Se contact, with a distance of 4.348 Å ($Q_W = 1.09$). In the other interchain arrangements the interchain contacts are considerably larger and the closest separations occur for the I–IV pair (Figure 1.6(c)) involving two C atoms from the donor Me groups, with a separation of 4.263 Å ($Q_W = 1.33$) in the case of $[\text{Fe}(\text{Cp}^*)_2][\text{Pt}(\text{tds})_2]$. However $[\text{Cr}(\text{Cp}^*)_2][\text{Pt}(\text{tds})_2]$ is not isostructural with these compounds, the intra and interchain arrangements are similar to those described above for $[\text{Fe}(\text{Cp}^*)_2][\text{Pt}(\text{tds})_2]$ [28].

The magnetic behavior of the compounds $[\text{Fe}(\text{Cp}^*)_2][\text{Pt}(\text{tdt})_2]$, $[\text{M}(\text{Cp}^*)_2][\text{Ni}(\text{tds})_2]$ and $[\text{M}(\text{Cp}^*)_2][\text{Pt}(\text{tds})_2]$ ($\text{M} = \text{Fe}$, Mn and Cr) is clearly dominated by the strong intrachain DA FM coupling, as can be seen by the high positive θ values (Table 1.3). The coexistence of an intrachain AFM interaction is responsible for the metamagnetic transitions, which are observed in several of those compounds, with $T_N = 2.1, 3.3, 5.7 \text{ K}$ and $H_C = 0.28, 3.95, 4.05 \text{ kG}$

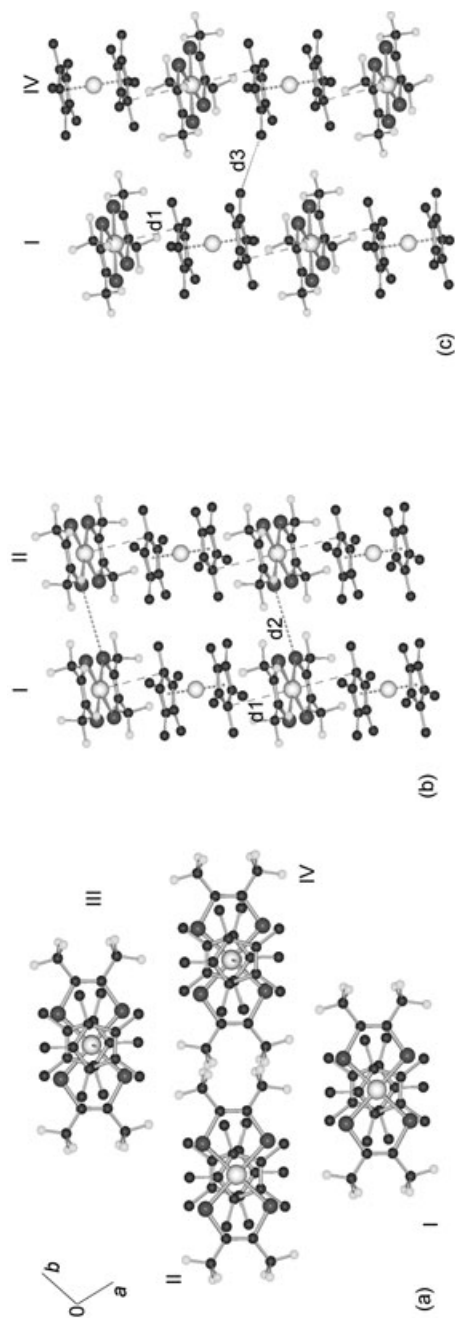


Fig. 1.6. (a) Perspective view of the crystal structure of $[\text{Fe}(\text{Cp}^*)_2][\text{Pt}(\text{tds})_2]$ along the chain direction. (b) Interchain arrangement of the pair I-II, d1 corresponds to the DA closest intrachain contact (3.826 Å, $Q_W = 0.98$) and d2 to the closest interchain contact (4.348 Å, $Q_W = 1.09$). (c) Interchain arrangement of the pair I-IV, d3 is the closest interchain contact (4.263 Å, $Q_W = 1.33$). Hydrogen atoms were omitted for clarity.

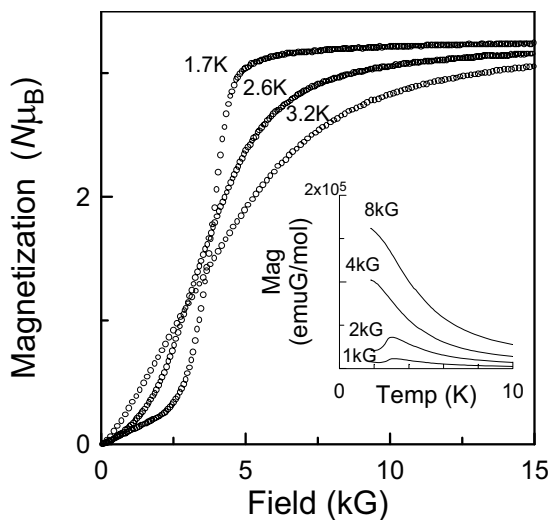


Fig. 1.7. Magnetization field dependence for $[\text{Fe}(\text{Cp}^*)_2][\text{Pt}(\text{tds})_2]$, at 1.7, 2.6 and 3.2 K. The inset shows the magnetization temperature dependence at 1, 2, 4 and 8 kG.

for $[\text{Mn}(\text{Cp}^*)_2][\text{Ni}(\text{tds})_2]$, $[\text{M}(\text{Cp}^*)_2][\text{Pt}(\text{tds})_2]$ ($\text{M} = \text{Fe}, \text{Pt}$) respectively. The magnetization field dependence at 1.7, 2.6 and 3.2 K for $[\text{Fe}(\text{Cp}^*)_2][\text{Pt}(\text{tds})_2]$ is shown in Figure 1.7, a sigmoidal behavior typical of metamagnetic behavior is observed for $T < T_N = 3.3 \text{ K}$ [26]. For low applied magnetic fields ($H < H_C$), a maximum in the magnetization temperature dependence can be observed, corresponding to an AFM transition, which is suppressed with fields $H > H_C$, as shown in the inset of Figure 1.7. The critical field temperature dependence obtained from the isothermal (closed symbols) and isofield (open symbols) measurements is shown in Figure 1.8.

In the compounds $[\text{Fe}(\text{Cp}^*)_2][\text{Pt}(\text{tdt})_2]$, $[\text{M}(\text{Cp}^*)_2][\text{Ni}(\text{tds})_2]$ and $[\text{M}(\text{Cp}^*)_2][\text{Pt}(\text{tds})_2]$ ($\text{M} = \text{Fe}, \text{Mn}$ and Cr) the Se–Se (or S–S) contacts, are expected to give rise to strong AFM interchain interactions, as the contacts are relatively short and there is a significant spin density on those atoms. The intrachain DA contacts (along c) and the interchain AA (Se–Se or S–S) contacts (along a) are expected to give rise to quasi-2D magnetic systems (ac plane), as the other interchain contacts are expected to give rise to much weaker magnetic interactions. The situation is quite distinct from that observed in the compounds $[\text{M}(\text{Cp}^*)_2][\text{Ni}(\text{edt})_2]$, $[\text{Fe}(\text{Cp}^*)_2][\text{Ni}(\text{tdt})_2]$ and $[\text{Mn}(\text{Cp}^*)_2][\text{M}'(\text{tdt})_2]$, where the interchain magnetic interactions are expected to be considerably more isotropic, and for these compounds the magnetic systems can be described as quasi-1D. The distinct dimensionality of the magnetic systems is reflected in the fast saturation observed in the isothermals, just above H_C , in the case of the salts with the quasi-2D magnetic systems, unlike the compounds presenting quasi-1D magnetic

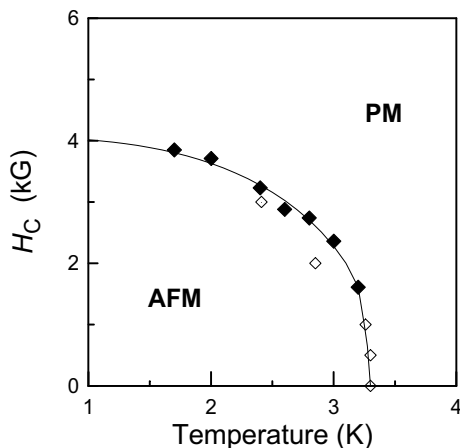


Fig. 1.8. Critical field dependence for $[\text{Fe}(\text{Cp}^*)_2][\text{Pt}(\text{tds})_2]$, where the closed and open symbols correspond to the data obtained with isothermal and isofield measurements respectively.

systems, where saturation occurs only at very high magnetic fields, when the temperature is not much lower than T_N [26].

In the case of $[\text{Cr}(\text{Cp}^*)_2][\text{Pt}(\text{tds})_2]$ metamagnetic behavior was also observed ($T_N = 5.2$ K), but a rather complicated phase diagram was obtained. Below T_N , two field induced transitions were observed to occur, and at 1.7 K the critical fields were 5 and 16 kG, respectively [28]. This is the first example of a metamagnetic transition on a $[\text{Cr}(\text{Cp}^*)_2]$ based ET salt and the low temperature phase diagram is still under study [28].

The analysis of the crystal structures, the magnetic behavior and atomic spin density calculations of several ET salts based on decamethylferrocenium and on metal-bis(dichalcogenate) acceptors with structures consisting of arrangements of parallel alternating DA linear chains, allowed a systematic study of the intra and interchain magnetic interactions [26]. In the case of these compounds a spin polarization is observed in the metallocenium donors but not in the acceptors described so far. The analysis of the intrachain contacts in the perspective of the McConnell I mechanism suggests the existence of intrachain FM coupling, through the contacts involving the metal or chalcogen atoms (positive spin density) from the acceptors and the C atoms (negative spin density) from the Cp ring of the donors, which shows good agreement with the experimental observations. A variety of interionic interchain contacts were observed in these ET salts, AA (Se–Se, S–S and C–C), DD (Me–Me) and DA (Me–S), and all these contacts were observed to lead to AFM interchain coupling. A strict application of the McConnell I model was not possible in the case of the interchain contacts, as the shortest contacts would involve mediation through H or F atoms, which are expected to present a very small spin density [26]. However the results regarding the nature of the interchain magnetic coupling would be compatible with that model if the contacts involving H or F atoms were neglected, as all the atoms involved in these contacts present a posi-